REAL-TIME ESTIMATION OF THE CAMERA PATH FROM A SEQUENCE OF INTRINSICALLY CALIBRATED PMD DEPTH IMAGES

Christian Beder, Ingo Schiller and Reinhard Koch

Computer Science Department
Christian-Albrechts-University Kiel
Hermann-Rodewald-Str. 3
D-24118 Kiel
Germany
{beder,rk}@mip.informatik.uni-kiel.de

KEY WORDS: Close Range Photogrammetry, 3D sensors, Computer Vision, Adjustment, Industrial measurement, PMD camera, Real-time Processing, Relative Orientation

ABSTRACT:

In recent years real time active 3D range cameras based on time-of-flight technology using the Photonic-Mixer-Device (PMD) have been developed. Those cameras produce sequences of low-resolution depth images at frame rates comparable to regular video cameras. Hence, spatial resolution is traded against temporal resolution compared to standard laser scanning techniques.

In this work an algorithm is proposed, which allows to reconstruct the camera path of a moving PMD depth camera. A constraint describing the relative orientation between two calibrated PMD depth images will be derived. It will be shown, how this constraint can be used to efficiently estimate a camera trajectory from a sequence of depth images in real-time.

The estimation of the trajectory of the PMD depth camera allows to integrate the depth measurements over a long sequence taken from a moving platform. This increases the spatial resolution and enables interactive scanning objects with a PMD camera in order to obtain a dense 3D point cloud.

1 INTRODUCTION

Real time active 3D range cameras based on time-of-flight technology using the Photonic-Mixer-Device (PMD) like the Zess MultiCam (cf. (Kraft et al., 2004)) depicted in figure 1 have been developed in recent years. Those cameras produce low-resolution depth images at high frame rates comparable to regular video cameras. Hence, spatial resolution is traded against temporal resolution in this systems compared to standard laser scanning techniques. The high frame rates make it also possible to move those PMD depth cameras around in space and acquire 3D data interactively. However, in order to make use of the measured 3D range data the trajectory of the camera has to be estimated. In this work an algorithm will be presented, that allows to estimate such a trajectory in real-time based solely on the depth measurements from a calibrated PMD depth camera.

Most previous work on estimating the trajectory of a moving PMD camera is based on external sensors other than the depth images themselves. Because the frame rates are comparable to regular video cameras, many people (cf. (Beder et al., 2007b), (Kuhnert and Stommel, 2006), (Streckel et al., 2007) and also (Prusak et al., 2007)) have combined the PMD camera with classical optical cameras and use classical photogrammetric techniques for the task of estimating the trajectory of the system. In (Huhle et al., 2007) a combined energy function using 3D point registration as well as intensity information from an attached optical camera is proposed for the task of estimating the trajectory. In contrast to this we use only the depth information from the PMD camera here.

Registration of point clouds is classically performed using the Iterative Closest Points (ICP) algorithm (cf. (Zhang, 1994)). This has been used for estimating the relative pose of PMD cameras in (Fuchs and May, 2007). However, while being very closely related to our approach, the ICP algorithm minimizes distances in 3D space. In contrast to our approach, this does not capture
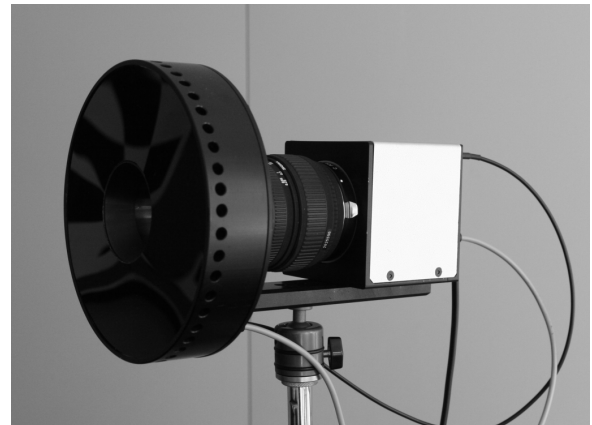

Figure 1: The Zess MultiCam PMD camera. Modulated infrared light is emitted from the front ring and the depth is measured using the Photonic Mixer Device behind it. The resolution is 64×48 pixels and the opening angle is approximately $18° \times 14°$.

the uncertainty structure of PMD depth images being a fixed 2D grid and measuring only depths. Assuming those depth measurements to be disturbed by Gaussian white noise our approach is the maximum-likelihood-estimate of the relative transformation. Furthermore, our approach directly makes use of the fixed 2D topology of the range image allowing efficient real-time processing of the data.

A crucial point for our algorithm to work is the accurate calibration of the PMD camera. Such calibration methods have been presented for instance in (Kahlmann et al., 2006) and (Lindner and Kolb, 2006). The calibration method we used has been presented in (Beder and Koch, 2007). The achievable accuracies of a current PMD camera have been studied in (Beder et al., 2007a).

This work is structured as follows. In the next section a geo-

metric model for a pair of calibrated PMD depth cameras will be proposed and a constraint between two such depth image views will be derived. Next it will be shown, how the Taylor expansion of the presented constraint can be efficiently computed from the range images and an efficient estimation scheme for computing the relative rotation and translation between two depth images will be presented. Finally we will show some results on real and synthetic image sequences using the proposed approach.

2 CAMERA MODEL

In the following the underlying geometric camera model for a pair of calibrated PMD depth camera will be presented. Therefore we will assume that the PMD depth image is rectified such that all non-linear distortions are compensated, i.e. lines in the scene are projected into lines in the image. Furthermore we will assume, that the remaining five linear calibration parameters are known and collected in the upper triangular matrix K_1. Assuming without loss of generality the coordinate system to be centered at the first reference camera, scene points project to an image position in this camera according to the following homogeneous equation (cf. (Hartley and Zisserman, 2003, p.157) and (Mugnier et al., 2004, p.225))

$$\mathbf{x}_1 \propto K_1 \boldsymbol{X} \tag{1}$$

In contrast to classical optical cameras, each pixel in a calibrated PMD image corresponds to a metric depth λ_1, so that the above equation may be inverted. Hence, the corresponding 3d point $\boldsymbol{X}$ is obtained for each depth pixel as

$$\boldsymbol{X} = \lambda_1 \frac{K_1^{-1}\mathbf{x}_1}{\sqrt{\mathbf{x}_1^\mathsf{T} K_1^{-T} K_1^{-1} \mathbf{x}_1}} \tag{2}$$

Now we consider a second PMD depth image taken from a different viewpoint. A scene point is projected to an image position according to the homogeneous equation (cf. (Hartley and Zisserman, 2003, p.157) and (Mugnier et al., 2004, p.225))

$$\mathbf{x}_2 \propto K_2 R^\mathsf{T}(\boldsymbol{X} - \boldsymbol{C}) \tag{3}$$

where the calibration parameters for this view are collected in the matrix K_2 and the position of the camera is given by a translation vector $\boldsymbol{C}$ and a rotation matrix R. This translation and rotation is about to be estimated in the following.

Again this equation is invertible, so that a 3d point is obtained from each depth pixel λ_2 according to

$$\boldsymbol{X} = \lambda_2 \frac{R K_2^{-1}\mathbf{x}_2}{\sqrt{\mathbf{x}_2^\mathsf{T} K_2^{-T} K_2^{-1} \mathbf{x}_2}} + \boldsymbol{C} \tag{4}$$

Setting equation (2) equal to equation (4) yields

$$\lambda_1 \frac{K_1^{-1}\mathbf{x}_1}{\sqrt{\mathbf{x}_1^\mathsf{T} K_1^{-T} K_1^{-1} \mathbf{x}_1}} = \lambda_2 \frac{R K_2^{-1}\mathbf{x}_2}{\sqrt{\mathbf{x}_2^\mathsf{T} K_2^{-T} K_2^{-1} \mathbf{x}_2}} + \boldsymbol{C} \tag{5}$$

Furthermore we substitute equation (2) into equation (3) yielding

$$\mathbf{x}_2 \propto K_2 R^\mathsf{T}\left(\lambda_1 \frac{K_1^{-1}\mathbf{x}_1}{\sqrt{\mathbf{x}_1^\mathsf{T} K_1^{-T} K_1^{-1} \mathbf{x}_1}} - \boldsymbol{C}\right) \tag{6}$$

Finally substituting equation (6) into equation (5) yields the condition

$$\lambda_1 \frac{K_1^{-1}\mathbf{x}_1}{\sqrt{\mathbf{x}_1^\mathsf{T} K_1^{-T} K_1^{-1} \mathbf{x}_1}} \tag{7}$$

$$= \lambda_2 \frac{\lambda_1 \dfrac{K_1^{-1}\mathbf{x}_1}{\sqrt{\mathbf{x}_1^\mathsf{T} K_1^{-T} K_1^{-1} \mathbf{x}_1}} - \boldsymbol{C}}{\sqrt{\lambda_1^2 - 2\lambda_1 \dfrac{\boldsymbol{C}^\mathsf{T} K_1^{-1}\mathbf{x}_1}{\sqrt{\mathbf{x}_1^\mathsf{T} K_1^{-T} K_1^{-1} \mathbf{x}_1}} + \boldsymbol{C}^\mathsf{T}\boldsymbol{C}}} + \boldsymbol{C}$$

Note, that λ_2 is dependent on $\mathbf{x}_2$ and hence on R and K_2 via equation (6). Next we will simplify this equation.

Denoting the normalized direction of the optical ray with

$$\boldsymbol{m}_1 = \frac{K_1^{-1}\mathbf{x}_1}{\sqrt{\mathbf{x}_1^\mathsf{T} K_1^{-T} K_1^{-1} \mathbf{x}_1}} \tag{8}$$

the condition simplifies to

$$(\lambda_1 \boldsymbol{m}_1 - \boldsymbol{C}) = \frac{\lambda_2}{\sqrt{\lambda_1^2 - 2\lambda_1 \boldsymbol{C}^\mathsf{T}\boldsymbol{m}_1 + \boldsymbol{C}^\mathsf{T}\boldsymbol{C}}}(\lambda_1 \boldsymbol{m}_1 - \boldsymbol{C}) \tag{9}$$

from which we finally deduce the following constraint

$$\lambda_2 = \sqrt{\lambda_1^2 - 2\lambda_1 \boldsymbol{C}^\mathsf{T}\boldsymbol{m}_1 + \boldsymbol{C}^\mathsf{T}\boldsymbol{C}} \tag{10}$$

This equation encapsulates the constraints a consistent pair of PMD depth images taken from a rigid scene must fulfill. In the following we will devise an algorithm, which uses this constraints for the estimation of the relative pose between two such PMD depth images. In the next section it will be shown, how this constraint may be linearized followed by a section describing how to estimate the relative translation and rotation using the constraint.

3 LINEARIZATION

We will now show, how the constraint (10) can be linearized in order to enable an efficient estimation scheme. Therefore we rewrite it as implicit equation

$$g = \lambda_2[\boldsymbol{x}_2] - f = 0 \tag{11}$$

with

$$f = \sqrt{\lambda_1^2 - 2\lambda_1 \boldsymbol{C}^\mathsf{T}\boldsymbol{m}_1 + \boldsymbol{C}^\mathsf{T}\boldsymbol{C}} \tag{12}$$

We start by looking at the first part of the equation being the 2d depth image $\lambda_2[\boldsymbol{x}_2]$. Because equation (6) gives $\mathbf{x}_2$ as a homogeneous 3d vector, we introduce the 2d normalization function

$$\boldsymbol{h}\left[\begin{pmatrix} u \\ v \\ w \end{pmatrix}\right] = \frac{1}{w}\begin{pmatrix} u \\ v \end{pmatrix} \tag{13}$$

which returns the corresponding Euclidean 2d vector, so that we can re-write $\lambda_2[\boldsymbol{x}_2] = \lambda_2[\boldsymbol{h}[\mathbf{x}_2]]$ in terms of the homogeneous 3d vector $\mathbf{x}_2$.

The Jacobian of the 2d normalization function $\boldsymbol{h}$ is given by (cf. (Beder, 2007, p.56))

$$\boldsymbol{J}_h[\mathbf{x}] = \frac{\partial \boldsymbol{h}[\mathbf{x}]}{\partial \mathbf{x}} = \frac{1}{w}\left(I_2 \quad -\frac{1}{w}\begin{pmatrix} u \\ v \end{pmatrix} \right) \tag{14}$$

so that the any derivative of the depth image λ_2 may be computed using the gradient depth image $\nabla \lambda_2$ and the correspond-

ing derivative of the homogeneous vector $\mathbf{x}_2$ by simply applying chain rule

$$\frac{\partial \lambda_2}{\partial \cdot} = \nabla \lambda_2[\boldsymbol{x}_2] J_h[\mathbf{x}_2] \frac{\partial \mathbf{x}_2}{\partial \cdot} \qquad (15)$$

Now using the Taylor expansion of the rotation (cf. (Förstner and Wrobel, 2004, p.53))

$$R \approx R_0 + S[\mathbf{r}] \qquad (16)$$

with the skew symmetric matrix

$$S\left[\begin{pmatrix} \omega \\ \phi \\ \kappa \end{pmatrix}\right] = \begin{pmatrix} 0 & -\kappa & \phi \\ \kappa & 0 & -\omega \\ -\phi & \omega & 0 \end{pmatrix} \qquad (17)$$

the partial derivatives of equation (6) after the parameters $\boldsymbol{r}$ and C as well as after the observations λ_1 are straightforward

$$\frac{\partial \mathbf{x}_2}{\partial C} = -K_2 R^\mathsf{T} \qquad (18)$$

$$\frac{\partial \mathbf{x}_2}{\partial \boldsymbol{r}} = K_2 S[\lambda_1 \boldsymbol{m}_1 - C] \qquad (19)$$

$$\frac{\partial \mathbf{x}_2}{\partial \lambda_1} = K_2 R^\mathsf{T} \boldsymbol{m}_1 \qquad (20)$$

and can be inserted into equation (15).

Finally we note that the derivatives of f are easily computed as

$$\frac{\partial f}{\partial C} = \frac{C^\mathsf{T} - \lambda_1 \boldsymbol{m}_1^\mathsf{T}}{f} \qquad (21)$$

$$\frac{\partial f}{\partial \boldsymbol{r}} = \mathbf{0}_3^\mathsf{T} \qquad (22)$$

$$\frac{\partial f}{\partial \lambda_1} = \frac{\lambda_1 - C^\mathsf{T} \boldsymbol{m}_1}{f} \qquad (23)$$

so that putting everything together the Taylor expansion of equation (11) at C, $\boldsymbol{r}$ and λ_1 is given by

$$g \approx g_0 + \boldsymbol{a}^\mathsf{T} \begin{pmatrix} \widehat{C} - C \\ \widehat{\boldsymbol{r}} - \boldsymbol{r} \end{pmatrix} + b(\widehat{\lambda_1} - \lambda_1) \qquad (24)$$

using the following Jacobians

$$\begin{aligned} \boldsymbol{a}^\mathsf{T} &= \nabla \lambda_2[\boldsymbol{x}_2] J_h[\mathbf{x}_2] K_2 \begin{pmatrix} -R^\mathsf{T} & S[\lambda_1 \boldsymbol{m}_1 - C] \end{pmatrix} \\ &\quad - \begin{pmatrix} \frac{C^\mathsf{T} - \lambda_1 \boldsymbol{m}_1^\mathsf{T}}{f} & \mathbf{0}_3^\mathsf{T} \end{pmatrix} \end{aligned} \qquad (25)$$

and

$$b = \nabla \lambda_2[\boldsymbol{x}_2] J_h[\mathbf{x}_2] K_2 R^\mathsf{T} \boldsymbol{m}_1 - \frac{\lambda_1 - C^\mathsf{T} \boldsymbol{m}_1}{f} \qquad (26)$$

Finally we introduce the observed depth $\overline{\lambda_1}$ and augment equation (24) as follows

$$g \approx g_0 + \boldsymbol{a}^\mathsf{T} \begin{pmatrix} \widehat{C} - C \\ \widehat{\boldsymbol{r}} - \boldsymbol{r} \end{pmatrix} + b(\widehat{\lambda_1} - \lambda_1 + \overline{\lambda_1} - \overline{\lambda_1}) \qquad (27)$$

Setting this augmented equation equal to zero yields the linearized constraint equation required for the estimation using the Gauss-Helmert-Model (cf. (Förstner and Wrobel, 2004, p.83))

$$\boldsymbol{a}^\mathsf{T} \widehat{\Delta \boldsymbol{p}} + b\hat{v} = c_g \qquad (28)$$

with the parameter update being

$$\widehat{\Delta \boldsymbol{p}} = \begin{pmatrix} \widehat{C} - C \\ \widehat{\boldsymbol{r}} - \boldsymbol{r} \end{pmatrix} \qquad (29)$$

the residual being

$$\hat{v} = \widehat{\lambda_1} - \overline{\lambda_1} \qquad (30)$$

and the contradiction being

$$c_g = -g_0 - b(\overline{\lambda_1} - \lambda_1) \qquad (31)$$

In the following section we will show, how this linearized constraint equation can be used to efficiently estimate the translation and rotation between the views.

4 ESTIMATION

In this section the linearized geometric model of the calibrated PMD depth image pair will be used to devise an efficient iterative estimation scheme for the unknown translation C and rotation R between the two views from the depth observations $\overline{\lambda_{1i}}$ given by the pixel values of the first PMD depth image.

We will assume that the motion between successive frames is small, so that we may begin with an initial linearization point

$$C = \mathbf{0}_3 \qquad (32)$$

and

$$\boldsymbol{r} = \mathbf{0}_3 \qquad (33)$$

If external knowledge about the motion is available, e.g. from external sensors, it could be used here as well. However, as the frame rate of current PMD cameras is at about 15 Hz, the above assumption is usually sufficient for initialization.

Furthermore we initialize the linearization point of the depth values with the observed values from the camera

$$\lambda_{1i} = \overline{\lambda_{1i}} \qquad (34)$$

Given a standard deviation σ_i for each observed depth value $\overline{\lambda_{1i}}$, the best linear unbiased estimate for the motion parameters may be obtained by iterating the following equations until convergence.

First the parameter update is computed as (cf. (Förstner and Wrobel, 2004, p.86))

$$\widehat{\Delta \boldsymbol{p}} = \left(\sum_{i=1}^{N} \frac{\boldsymbol{a}_i \boldsymbol{a}_i^\mathsf{T}}{\sigma_i^2 b_i^2} \right)^{-1} \sum_{i=1}^{N} \frac{\boldsymbol{a}_i c_{g_i}}{\sigma_i^2 b_i^2} \qquad (35)$$

Observe, that for this normal equation matrix to be non-singular, sufficient depth gradient has to be present in the images.

Using this parameter update we may also update the estimated residuals as

$$\widehat{v_i} = \frac{c_{g_i} - \boldsymbol{a}_i^\mathsf{T} \widehat{\Delta \boldsymbol{p}}}{b_i} \qquad (36)$$

From this the new linearization point is obtained as

$$\begin{pmatrix} C^{(\nu+1)} \\ \boldsymbol{r}^{(\nu+1)} \end{pmatrix} = \begin{pmatrix} \widehat{C}^{(\nu)} \\ \widehat{\boldsymbol{r}}^{(\nu)} \end{pmatrix} = \begin{pmatrix} C^{(\nu)} \\ \boldsymbol{r}^{(\nu)} \end{pmatrix} + \widehat{\Delta \boldsymbol{p}} \qquad (37)$$
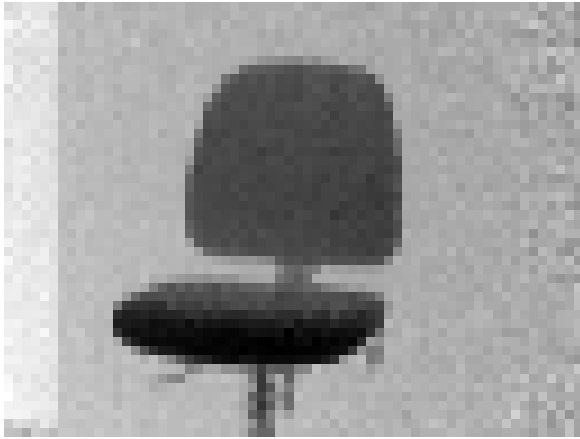
Figure 2: First depth image of the test sequence showing the distances to an office chair at approximately 4m.

and

$$\lambda_{1\,i}^{(\nu+1)} = \widehat{\lambda}_{1\,i}^{(\nu)} = \overline{\lambda_{1\,i}} + \widehat{v_i} \tag{38}$$

This process is iterated using the updated Jacobians until convergence yielding an estimate for the translation $\widehat{C}^{(\nu)}$ and the rotation $\widehat{r}^{(\nu)}$.

Finally the covariance matrix of those estimated parameters is given by (cf. (Förstner and Wrobel, 2004, p.86))

$$\Sigma = \left(\sum_{i=1}^{N} \frac{a_i a_i^{\mathsf{T}}}{\sigma_i^2 b_i^2} \right)^{-1} \tag{39}$$

Given an image sequence, the translation and rotation can be estimated between successive frames as shown above. Those transformation can now be accumulated over a whole sequence of depth images yielding the trajectory of the depth camera.

5   RESULTS

In order to demonstrate the feasibility of the above approach we took an image sequence with a ZESS MultiCam PMD camera depicted in figure 1. This camera produces depth measurements at a resolution of 64×48 pixels at 15 Hz. The opening angle of the optics is approximately $18° \times 14°$. The camera was calibrated using the approach presented in (Beder and Koch, 2007).

The sequence comprises of 100 depth images of an office chair approximately $4m$ in front of the camera. The first image of the sequence is depicted in figure 2 the last picture of the sequence is depicted in figure 3.

In figure 4 the 3D points and camera position from the first image are shown. The 3D point cloud comprises of only $64 \times 48 = 3072$ points. As the camera moves each new frame yields 3072 new 3D points. The point cloud remains registered, as the trajectory is estimated along the sequence. In figure 5 the 3D point cloud together with the camera trajectory after 20 frames is shown. The final point cloud and camera trajectory is depicted in figure 6. The 3D point cloud now comprises of $100 \times 3072 = 307200$ points after approximately 7 seconds at 15 Hz.

It can be seen, that by integrating measurements over time the spatial resolution can be increased by reducing the temporal resolution. Because the PMD camera needs to be moved to achieve
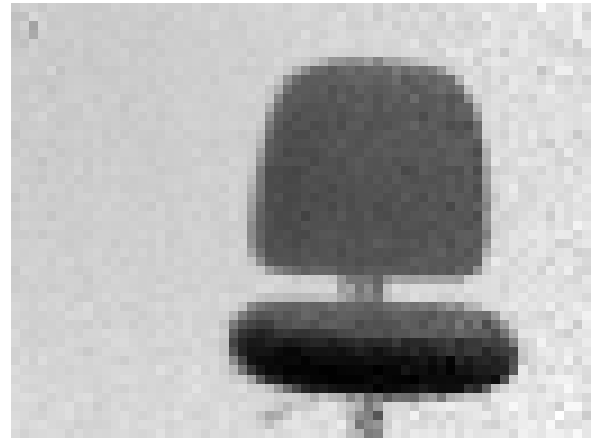

Figure 3: Last image of the sequence comprising of 100 images. The camera was moved to the left and kept focused on the office chair.

Figure 4: Camera pose and 3D point cloud obtained only from the first depth image. The image is showing a view of the office chair from behind and toward the camera. The point cloud is still very sparse comprising of only 3072 points.
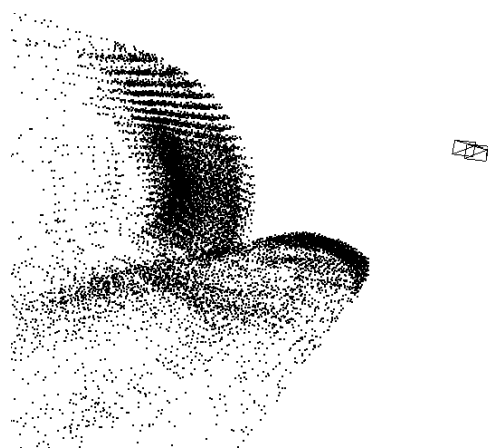

Figure 5: Intermediate 3D point cloud and camera trajectory. The point cloud has become more dense due to the movement of the PMD camera.
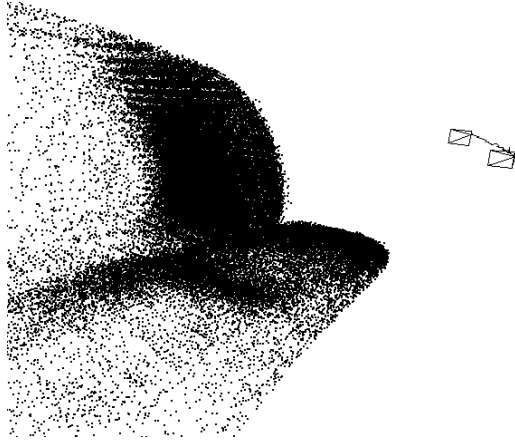
Figure 6: Final 3D point cloud after 100 images now comprising of 307200 points. The camera trajectory is shown as well.
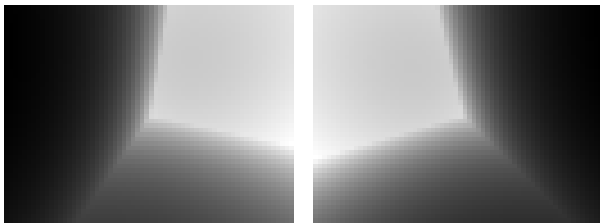

Figure 7: First and last depth image of the synthetic test sequence. It shows a rectangular corner at a distance of $3m$ in front of the camera, which is moved $4m$ to the right keeping the corner centered.

this goal, the trajectory has to estimated in order to keep the 3D points registered consistently.

The trajectory estimation proposed here is based on subsequent estimation and accumulation of the camera movement. In contrast to an overall adjustment this approach enables real-time on-line processing of the sequence but also leads to the accumulation of errors. To quantify this effect of error accumulation we generated a synthetic test sequence comprising of 200 images of a single rectangular corner. The corner was set at a distance of $3m$ in front of the camera and the camera was moved over 100 frames $4m$ to the left keeping the corner centered. Then the camera was moved back on the same path for another 100 frames, so that the final position was again at the starting point. The first and last depth image of the half camera path are shown in figure 7 and the 3D setup of the first half of the sequence is depicted in figure 8.

Now we added Normal distributed white noise to the depth images of the sequence and compared the estimated starting position and the end position of the cameras, which should coincide. In figure 9 the distances between the first and last camera pose are plotted against the variance of the image noise. As expected the accumulated error after 200 frames increases with increasing depth image noise. It can be seen, that for noise levels below $\sigma^2 = (15cm)^2 = 0.0225m^2$ the position error is below $10cm$ and the rotation error is below $5°$ for an object at $3m$ distance to the camera. This accuracy seems reasonable for our real-time approach, but could be improved by an overall adjustment also incorporating other sensors than the PMD depth camera.

6 CONCLUSION

We have presented an algorithm for the real-time estimation of the trajectory of a freely moving calibrated PMD depth camera.
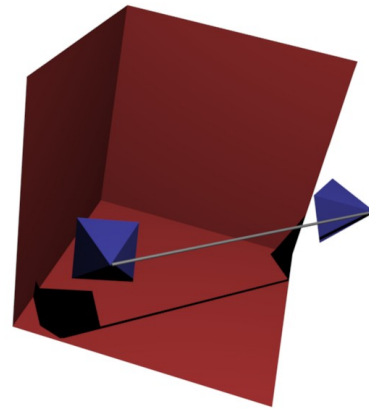

Figure 8: The 3D setup of the synthetic corner test sequence. The corner is $3m$ in front of the camera. Then the camera was moved to the right $4m$ keeping the corner centered and then back again, so that the final pose of the camera should coincide with the first.
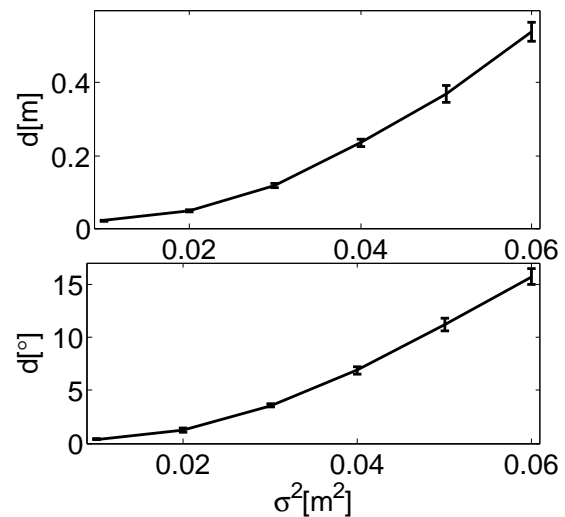

Figure 9: Distances of the first and last frame of the synthetic test sequence plotted against the variance of the image noise. *Top:* Distance between the projection centers of the two cameras. *Bottom:* Angular distance between the viewing directions of the two cameras.

A constraint between two such calibrated depth images has been derived and it has been shown, how this constraint can be used to efficiently compute the maximum-likelihood-estimate of the relative translation and rotation between the views. Results on real-time interactive acquisition of 3D data using a freely moving PMD camera have been presented. By estimating the trajectory and thereby registering the acquired 3D data the high temporal resolution of the PMD camera allows to interactively acquire dense 3D point clouds.

The major drawback of the presented approach relying solely on the depth data is the fact, that sufficient depth gradient has to be present in the images. As PMD cameras have to actively illuminate the scene, their field of view is usually designed to be very narrow so that it is quite likely, that no scene structure is visible in the current view. In this case our approach fails. Furthermore, the noise level of current PMD cameras is still very high. This poses major difficulties for our approach, because we assume that the gradient depth image can be computed, which might turn out to be very difficult for low-resolution images with bad signal-to-noise ratio.

Our future research will aim at circumventing those drawbacks. For instance the presented approach is very well suited to be integrated into a Kalman filter. This would allow to smooth the estimated trajectories using a prediction model and thereby also overcome regions of low depth gradient. Furthermore, as our approach is based on the maximum-likelihood-estimation using the Gauss-Helmert-Model, this allows to integrate other sensors such as video cameras and inertial sensors in a straightforward and mathematical rigorous manner.

REFERENCES

Beder, C., 2007. Grouping Uncertain Oriented Projective Geometric Entities with Application to Automatic Building Reconstruction. PhD thesis, Photogrammetry Department, Institute for Geodesy and Geoinformation, Bonn University, Germany, Nussallee 15, 53115 Bonn, Germany.

Beder, C. and Koch, R., 2007. Calibration of focal length and 3d pose based on the reflectance and depth image of a planar object. In: Proceedings of the DAGM Dyn3D Workshop, Heidelberg, Germany.

Beder, C., Bartczak, B. and Koch, R., 2007a. A Comparison of PMD-Cameras and Stereo-Vision for the Task of Surface Reconstruction using Patchlets. In: IEEE/ISPRS Workshop BenCOS, Minneapolis, MN.

Beder, C., Bartczak, B. and Koch, R., 2007b. A combined approach for estimating patchlets from PMD depth images and stereo intensity images. In: F. Hamprecht, C. Schnörr and B. Jähne (eds), Proceedings of the DAGM 2007, LNCS, Springer, pp. 11–20.

Förstner, W. and Wrobel, B., 2004. Mathematical concepts in photogrammetry. In: J.C.McGlone, E.M.Mikhail and J.Bethel (eds), Manual of Photogrammetry, Fifth Edition, ASPRS, pp. 15–180.

Fuchs, S. and May, S., 2007. Calibration and registration for precise surface reconstruction with tof cameras. In: Proceedings of the DAGM Dyn3D Workshop, Heidelberg, Germany.

Hartley, R. I. and Zisserman, A., 2003. Multiple View Geometry in Computer Vision, Second Edition. Cambridge University Press, ISBN: 0521623049.

Huhle, B., Jenke, P. and Strasser, W., 2007. On-the-fly scene acquisition with a handy multisensor-system. In: Proceedings of the DAGM Dyn3D Workshop, Heidelberg, Germany.

Kahlmann, T., Remondino, F. and Ingensand, H., 2006. Calibration for increased accuracy of the range imaging camera SwissrangerTM. In: IEVM06.

Kraft, H., Frey, J., Moeller, T., Albrecht, M., Grothof, M., Schink, B., Hess, H. and Buxbaum, B., 2004. 3d-camera of high 3d-frame rate, depth-resolution and background light elimination based on improved pmd (photonic mixer device)-technologies. In: 6th International Conference for Optical Technologies, Optical Sensors and Measuring Techniques (OPTO 2004).

Kuhnert, K. and Stommel, M., 2006. Fusion of stereo-camera and PMD-camera data for real-time suited precise 3d environment reconstruction. In: IEEE/RSJ International Conference on Intelligent Robots and Systems (IROS).

Lindner, M. and Kolb, A., 2006. Lateral and depth calibration of PMD-distance sensors. In: International Symposium on Visual Computing (ISVC06), Vol. 2, Springer, pp. 524–533.

Mugnier, C. J., Förstner, W., Wrobel, B., Paderes, F. and Munjy, R., 2004. The mathematics of photogrammetry. In: J.C.McGlone, E.M.Mikhail and J.Bethel (eds), Manual of Photogrammetry, Fifth Edition, ASPRS, pp. 181–316.

Prusak, A., Melnychuk, O., Schiller, I., Roth, H. and Koch, R., 2007. Pose estimation and map building with a pmd-camera for robot navigation. In: Proceedings of the DAGM Dyn3D Workshop, Heidelberg, Germany.

Streckel, B., Bartczak, B., Koch, R. and Kolb, A., 2007. Supporting structure from motion with a 3d-range-camera. In: Scandinavian Conference on Image Analysis (SCIA07).

Zhang, Z., 1994. Iterative point matching for registration of free-form curves and surfaces. International Journal of Computer Vision 13(2), pp. 119–152.